

Simulated U.S. Drought Response to Interannual and Decadal Pacific SST Variability

ROBERT J. BURGMAN AND YOUNKYOUNG JANG

Department of Earth and Environment, Florida International University, Miami, Florida

(Manuscript received 1 April 2014, in final form 28 January 2015)

ABSTRACT

Idealized atmospheric general circulation model (AGCM) experiments by the U.S. Climate Variability and Predictability Program (CLIVAR) Drought Working Group were used in order to study the influence of natural modes of sea surface temperature (SST) variability in the Pacific on drought in the contiguous United States. The current study expands on previous results by examining the atmospheric response of three AGCMs to three different patterns of the idealized Pacific SST anomalies that operate on different time scales: low-frequency (decadal), high-frequency (interannual), and a pan-Pacific pattern that retains characteristics of interannual and decadal variability. While forcing patterns are generally similar in appearance, results indicate that differences in the relative amplitude of the equatorial and extratropical components of the SST forcing are sufficient to give rise to differing teleconnections, leading to regional differences in the amplitude and significance of the precipitation response. Results indicate that the differences in simulated drought response between AGCMs to different cool-phase (La Niña-like) SST patterns are determined by model sensitivity to changes in the relative amplitude of the equatorial and extratropical components of the SST forcing, the strength of the land–atmosphere coupling, and by the amplitude of internal atmospheric variability. Results indicate that the northwestern United States and Great Plains regions are particularly sensitive to the extratropical component of the SST forcing. Evidence is also found that when the cool-phase patterns of SST combine, as they have in recent years, constructive interference leads to an enhanced drought response over the Great Plains.

1. Introduction

The recent multiyear drought in California and the Great Plains region coincides with an extended period of arid conditions over much of the contiguous United States that began in 1999, punctuated by more severe regional droughts in 1999, 2002, 2006, 2008, and 2011. In 2012, the U.S. drought monitor declared moderate to extreme drought conditions covered 64% of the contiguous United States, the most extensive drought to affect the United States since the “Dust Bowl” of the 1930s. The resulting widespread harvest failures and reduced cattle inventories affected meat and dairy prices. Estimates put the cost of the 2012 drought and associated heat wave in the tens of billions of U.S. dollars. Comparable periods of persistent drought were

recorded in the Great Plains region in the 1950s and the 1930s (the aforementioned Dust Bowl drought) and during several decades of the nineteenth century ([Herweijer et al. 2006; Herweijer and Seager 2008](#)). Further, analysis of proxy climate records and paleo-modeling studies indicates that similar periods of persistent U.S. drought have occurred over the past 1000 yr ([Woodhouse and Overpeck 1998; Herweijer and Seager 2008; Seager et al. 2008; Burgman et al. 2010](#)).

Clearly such extreme drought events have tremendous societal and economic impacts on the United States. Understanding the mechanisms and probability for drought onset, persistence, and intensity is paramount for decision makers, who must assess potential impacts and management options. For example, the decision-making processes will significantly depend on whether the recent droughts in the southwestern and central United States were due to natural climate variability or were due to external forcing of the climate system. Were the U.S. drought conditions of the past decade due to climate change, natural variability, or simply stochastic internal variability? If they were associated with natural variability, where was the signal coming from? Can future droughts be predicted? If there is

Denotes Open Access content.

Corresponding author address: Robert Burgman, Florida International University, 11200 SW 8th St., Miami, FL 33199.
E-mail: rburgman@fiu.edu

long-term predictability, the “memory” for this predictability resides with the global oceans, but precisely how the global oceans influence observed North American drought remains unresolved.

Important factors influencing North American hydroclimate include extratropical and tropical Pacific SSTs, SSTs in the North Atlantic, changes in storm tracks, shifts in the subtropical highs in the Atlantic and Pacific, changes in the Great Plains low-level jet, and land surface processes (Ropelewski and Halpert 1986; Trenberth et al. 1988; Enfield et al. 2001; Hu and Feng 2002; Barlow et al. 2001; Trenberth and Guillemot 1996; Higgins et al. 1997; Koster et al. 2006). The meteorological conditions associated with persistent droughts are well documented (i.e., Namias 1955; Trenberth and Guillemot 1996; Mo et al. 1997; Trenberth et al. 1998; Thompson and Wallace 1998; Nigam et al. 1999; Schubert et al. 2004a,b; Hoerling and Kumar 2003; Seager et al. 2003, 2005; Wu and Kinter 2009; Seager et al. 2010), though the mechanisms are not well understood. There is wide acceptance of the role of the tropical Pacific in forcing precipitation changes over North America via “teleconnections” that rely on the propagation of Rossby waves in Boreal winter. Recent research by Seager et al. (2003, 2010) also points to a more persistent zonally symmetric atmospheric response to tropical warming that involves equatorward shifts in the subtropical jets and transient eddies and tropospheric cooling in the middle latitudes that drive anomalous ascent. For anomalously cool tropical Pacific SSTs, a poleward shift in the subtropical jets and transient eddies leads to anomalous descent and warming in the middle latitudes and dry conditions over much of the contiguous United States. To better understand the relationship between SSTs and drought, modeling agencies have collaborated on atmospheric modeling projects that provide valuable data to climate researchers (Gates et al. 1999).

In addition to large modeling efforts aimed at understanding the atmospheric response to time-varying observed SSTs, several studies have used more idealized model configurations to elucidate the relative roles of SSTs in different basins or in different regions within a particular ocean basin on regional and remote precipitation variability. It is important to note that because the SST anomaly (SSTA) patterns are fixed with respect to time in these simulations, the AGCMs do not capture important aspects of the observed seasonality of the SST anomalies. This is especially important when considering variability in the tropical Pacific associated with the El Niño–Southern Oscillation (ENSO), which tends to peak in the boreal winter season. However, idealized “fixed SST” methodologies have been used to great effect in identifying the relative roles of regional SST

forcing on remote atmospheric response. Latif and Barnett (1994) forced an ensemble of atmospheric general circulation models (AGCMs) with the leading mode of North Pacific SST variability in perpetual January simulations to show that the weak Aleutian low extreme of the Pacific–North American (PNA) pattern could be reproduced without tropical SST forcing. Barsugli and Sardeshmukh (2002) incorporated SST anomaly “patches,” arrayed separately at 42 locations throughout the tropical Pacific in perpetual January simulations to identify AGCM sensitivities with regards to leading patterns of variability, such as the PNA pattern. The authors found that the PNA index was sensitive to tropical SSTs primarily in the Niño-4 region, though they also determined that individual centers of action within the PNA pattern (e.g., positive heights over western Canada) were sensitive to SSTs in different locations.

Schubert et al. (2004a) forced the National Aeronautics and Space Administration’s (NASA) Seasonal-to-Interannual Prediction Project (NSIPP) AGCM with both global observed SST and with a fixed (with respect to time) pan-Pacific SST pattern and found that the Great Plains consistently experienced meteorological drought on low-frequency time scales when the tropical eastern Pacific was relatively cold for extended periods. Hoerling and Kumar (2003) performed similar prescribed (time independent) SST experiments focusing in different simulations on the relative roles of the cool eastern tropical Pacific versus warm western Pacific and Indian Ocean tropical SST anomalies. The authors argued that the SST in these two regions constructively interfere with each other to produce the “perfect” ocean for the 1998–2002 midlatitude drying throughout North America, southern Europe, and southwest Asia.

Recently the relationship between dominant SST patterns and precipitation over the United States was studied by the U.S. Climate Variability and Predictability Program (CLIVAR) Drought Working Group (DWG) (Schubert et al. 2009; Findell and Delworth 2010; Mo et al. 2009; Wang et al. 2010; Hu et al. 2011). In this multiagency atmospheric modeling effort, Pacific, Atlantic, and global warming trend SSTA patterns were prescribed as persistent forcing in several different configurations [e.g., warm–neutral–cold Pacific combined with warm–neutral–cold Atlantic; see Schubert et al. (2009)] to investigate the influence of SSTs on precipitation over the United States. To date, the studies from this modeling effort have focused on a baseline Pacific SST pattern that has amplitude on the equator associated with observed interannual variability associated with ENSO in addition to amplitude in the extratropics associated with multidecadal variability [i.e., the interdecadal Pacific oscillation (IPO; Power et al. 1999) and Pacific decadal oscillation

(PDO; Mantua et al. 1997)]. Further simulations were carried out with the low-frequency (longer than 6 yr) and high-frequency Pacific patterns separated; however, these simulations were not performed by all participating agencies and, thus, drew less attention.

In this paper, we expand on previous studies by focusing on AGCM simulations where the decadal and interannual signals are effectively separated in order to examine how the Pacific SSTAs associated with different time scale variability impact hydroclimate over the contiguous United States, with a particular focus on the differences in amplitude of the equatorial and midlatitude SST anomalies and precipitation over the Great Plains region. The results of the two decomposed (high frequency and low frequency) Pacific SST forcing simulations are compared with the previously examined Pacific forcing simulation [cold Pacific pattern with neutral Atlantic conditions and no global trend signal (PcAn)], where the amplitudes of equatorial and midlatitude SSTAs are relatively large. We focus on the differences in the atmospheric response to the differing forcing patterns within each model and between the models for each forcing pattern. In section 2, we identify the AGCMs used in the study and describe the observational data and modeling methodology used in this study. In section 3, we describe the results of our analysis. In section 4, we summarize the results and discuss the implications of the analysis.

2. Models, modeling methodology, and data

Idealized AGCM simulations performed by members of the U.S. CLIVAR DWG were used in this study. The low-frequency (LF) and high-frequency (HF) AGCM simulations of interest for this study were carried out by three of the five agencies that contributed AGCM data to the DWG in addition to the baseline simulations noted above. The three models are:

- 1) The NASA Global Modeling and Assimilation Office (GMAO) NSIPP, version 1 (NSIPP1) AGCM at $3^\circ \times 3.75^\circ$, L34 resolution (Bacmeister et al. 2000; Schubert et al. 2002).
- 2) The National Oceanic and Atmospheric Administration's (NOAA) Climate Prediction Center Global Forecast System (GFS) AGCM at $2^\circ \times 2^\circ$, L64 resolution (Campana and Caplan 2005).
- 3) NOAA's Geophysical Fluid Dynamics Laboratory (GFDL) Atmosphere Model, version 2.1 (AM2.1), AGCM at $2^\circ \times 2.5^\circ$, L24 resolution (Delworth et al. 2006).

For the DWG AGCM simulations, idealized SST anomaly patterns are fixed in time and superimposed on climatologically varying SSTs derived from the Hadley

Centre Sea Ice and Sea Surface Temperature dataset (HadISST; Rayner et al. 2003) for the period 1901–2004. The SST pattern for the Pacific (PcAn; Fig. 1a) comes from the baseline experiments, where the patterns were derived by performing rotated empirical orthogonal function (REOF) analysis on annual mean global HadISST anomalies. The Pacific pattern used in this study was REOF2 (20.5% variance explained), the global warming trend was REOF1 (27.2% variance explained), and Atlantic pattern was REOF3 [5.8% variance explained; see Schubert et al. (2009), their Fig. 1]. Note that the principal component (PC) time series associated with the PcAn pattern in Fig. 1a captures the interannual variability of ENSO in addition to variability on decadal time scales.

The Drought Working Group also produced patterns of SST anomalies associated with the low-frequency and high-frequency tropical Pacific SST variability. The low-frequency cold (LFC) and high-frequency cold (HFc) patterns are shown in Figs. 1b and 1c, respectively. To accomplish this, monthly anomalies were filtered using a 6-yr recursive low-pass filter (as in Zhang et al. 1997) to filter out interannual and shorter time scales; the high-pass data were obtained by subtracting the low-pass anomalies from the unfiltered data. REOF analysis of the low-pass (c) monthly anomalies produced the LFC pattern as REOF2 (15% variance explained; REOF1 captured the warming trend) and REOF analysis of the high-pass data produced the HFc pattern as REOF1 (16.9% variance explained). The associated PC time series for the LFC and HFc patterns clearly illustrate the separation of the interannual and decadal signals with large-scale Pacific “regime shifts” evident in the 1940s, 1970s, and late 1990s for the LFC pattern (Zhang et al. 1997; Deser et al. 2004; Burgman et al. 2008a) and individual ENSO events in 1982/83, 1988/89, and 1997/98 highlighted for the HFc pattern.

We note that the methodology of the DWG and previous studies using idealized decadal SST patterns, by design, treat the SST pattern in Fig. 1b as an independent mode of variability. There is considerable debate in the literature as to the relationship between the slowly varying (multidecadal) Pacific “mean state” and ENSO. Kirtman and Schopf (1998) found that changes in the amplitude and predictability of ENSO were tied to decadal changes in the background mean state of the tropical Pacific in an intermediate coupled model, though the source of the mean state changes was unclear. Fedorov and Philander (2000) used a simple coupled model to show that ENSO frequency and growth rate were also modulated by changes in the mean trade wind intensity, thermocline depth, and thermocline gradient. Schopf and Burgman (2006) presented a simple kinematic mechanism with which one could recreate such apparent changes in the multidecadal mean state,

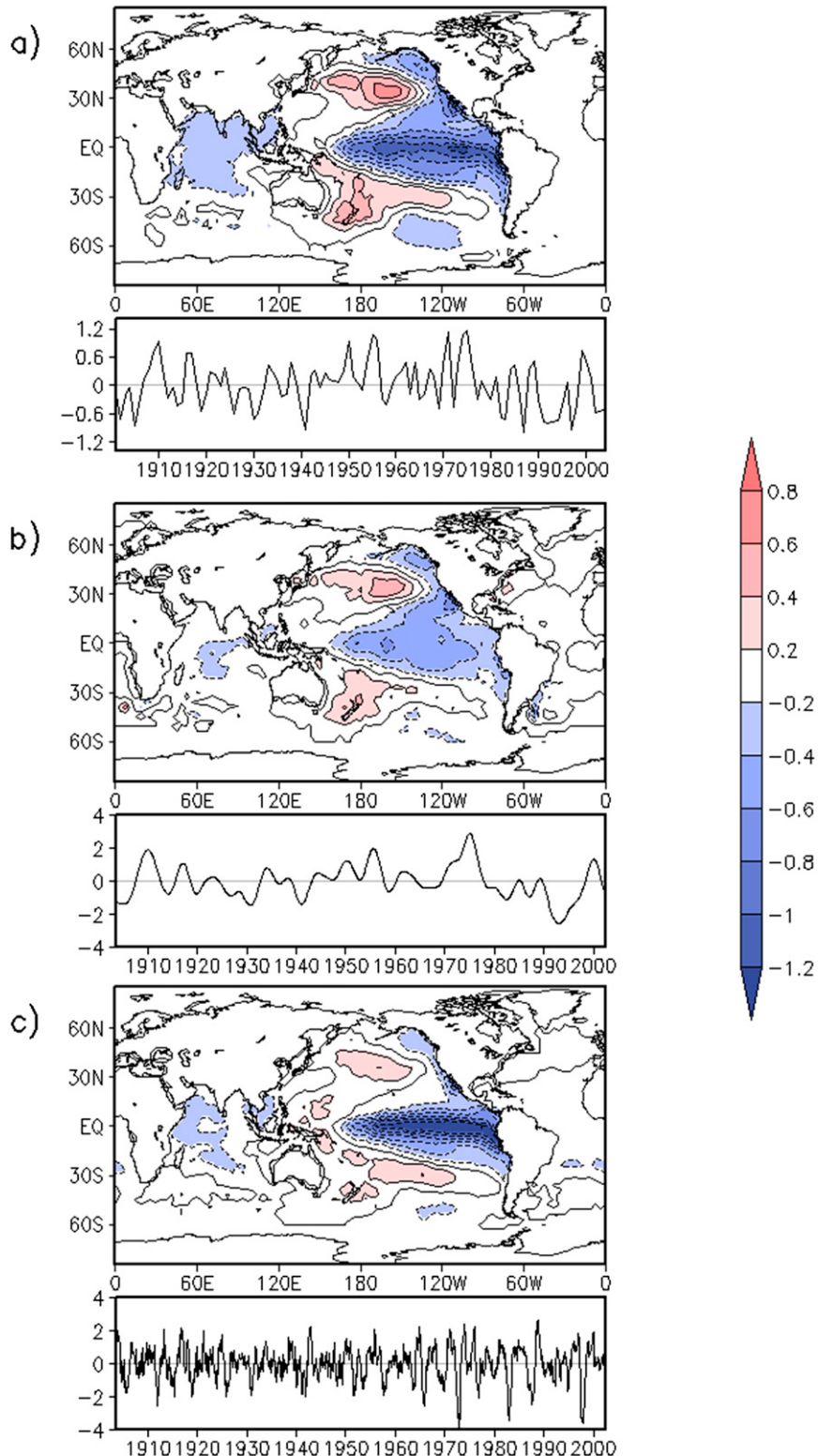


FIG. 1. The SST anomaly patterns ($^{\circ}\text{C}$) used in forcing for experiments with principal components: (a) PcAn, (b) LFc, and (c) HFc. The top panels are the idealized anomaly patterns of each type and the bottom panels are the climatologically varying SSTs by years.

as measured by the Eulerian mean, by introducing an oscillation to a nonlinear SST profile like the one observed in the equatorial Pacific. The results suggest that multidecadal warming (cooling) in eastern (western) Pacific SSTs described in previous studies may be attributable to changes in ENSO variance. Newman et al. (2003) argued that the PDO is dependent upon ENSO on all time scales, where the PDO is a consequence of a “reddened” ENSO response. Burgman et al. (2008b) used a hybrid coupled model with prescribed stochastic variability in the surface winds to show that low-frequency changes in the tropical Pacific mean state modulated ENSO amplitude and predictability while the mean state changes in the equatorial Pacific were driven by stochastic variability in the zonal winds.

The patterns of the anomalies are similar in a broad sense (spatial correlations for P_cAn and LFc, $r = 0.93$; P_cAn and HFc, $r = 0.9$; and LFc and HFc, $r = 0.79$); however, the amplitude of the equatorial (midlatitude) anomalies differ by up to 1°C (0.3°C) between the different patterns. In addition to the Pacific pattern used in the baseline DWG simulations, Fig. 1b shows the well-known pattern of Pacific decadal variability with reduced amplitude in the tropical latitudes, while the HFc pattern (Fig. 1c) has minimal amplitude in the middle latitudes. The LFc pattern (Fig. 1b) differs from the P_cAn pattern (Fig. 1a), with smaller amplitude in the equatorial eastern and central Pacific while retaining similar amplitude in the middle latitudes, representing decadal variability. The residual pattern (HFc in Fig. 1d) differs from the P_cAn pattern with larger amplitude in the equatorial Pacific and weaker amplitude in the western equatorial Pacific, the eastern subtropics, and middle latitudes. Note that, because of the methodology for deriving the patterns in Figs. 1a–c, the P_cAn pattern in Fig. 1a is not equivalent to the sum of the LFc and HFc patterns in Fig. 1b and Fig. 1c.

The GFDL AM2.1 and NASA NSIPP1 simulations were run for 50 yr and the NCEP GFS for 35 yr. The AGCM responses to the idealized SSTAs were obtained from the mean differences between the forced run and the control run, where no anomalous forcing was prescribed to the annual cycle of global SSTs [Pacific neutral and Atlantic neutral (PnAn)]. We focus in this study on cold Pacific conditions, which have been shown to cause arid conditions in the United States (McCabe et al. 2004; Mo et al. 2009; Schubert et al. 2009; Findell and Delworth 2010). We recognize that the Atlantic multidecadal SSTAs play a significant part in long-term predictability of U.S. drought (McCabe et al. 2004; Enfield et al. 2001); however, our focus in this study is Pacific phenomena, so the global temperature trend and Atlantic SSTA pattern are not considered. For the purposes of the regional analysis in this

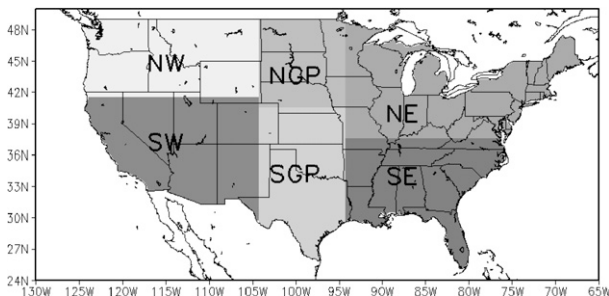


FIG. 2. The regions of the United States used to form averages in Figs. 4 and 5.

study, the contiguous United States is divided into six subregions (see Fig. 2); the northern–southern western United States, the northern–southern Great Plains, and the northern–southern eastern United States. The specified subregions were chosen to follow the regional analysis of Schubert et al. 2009 for consistency and approximate the U.S. climate divisions with some modifications for expediency. Values over the ocean are not considered in the analysis.

Observational estimates of precipitation were obtained from Global Precipitation Climatology Project (GPCP) monthly precipitation, combined with observations and satellite products at NOAA (Adler et al. 2003).

3. Results

a. Annual mean AGCM precipitation response

Figure 3 shows the annual mean precipitation response for three AGCMs to the three different forcing patterns shown in Fig. 1. The AM2.1 AGCM precipitation response (Figs. 3a,d,g) is characterized by an expansive area of negative anomalies reaching from the southwestern United States to the Midwest. In the Pacific Northwest, the precipitation response is positive, consistent with observational and modeling studies of La Niña-like SSTA conditions (e.g., Higgins et al. 1997; McCabe et al. 2004; Wang et al. 2010). The AM2.1 precipitation response is robust and comparable in all of the forcing experiments with similar amplitude across all experiments in the northwestern United States (NW). The largest negative anomalies in the Great Plains and U.S. Southeast are found in the HFc simulation and P_cAn simulation, respectively. The annual mean NSIPP1 precipitation response (Figs. 3b,e,h) is largest in the Great Plains, the U.S. Southeast, and in the U.S. Northwest, with the largest amplitude seen in the P_cAn simulation. The amplitude of the NSIPP1 response in the U.S. Northwest and Great Plains subregions is smallest in the HFc simulation, while the amplitude of the response in the southeastern United States is smallest in the LFc simulation. The GFS-simulated

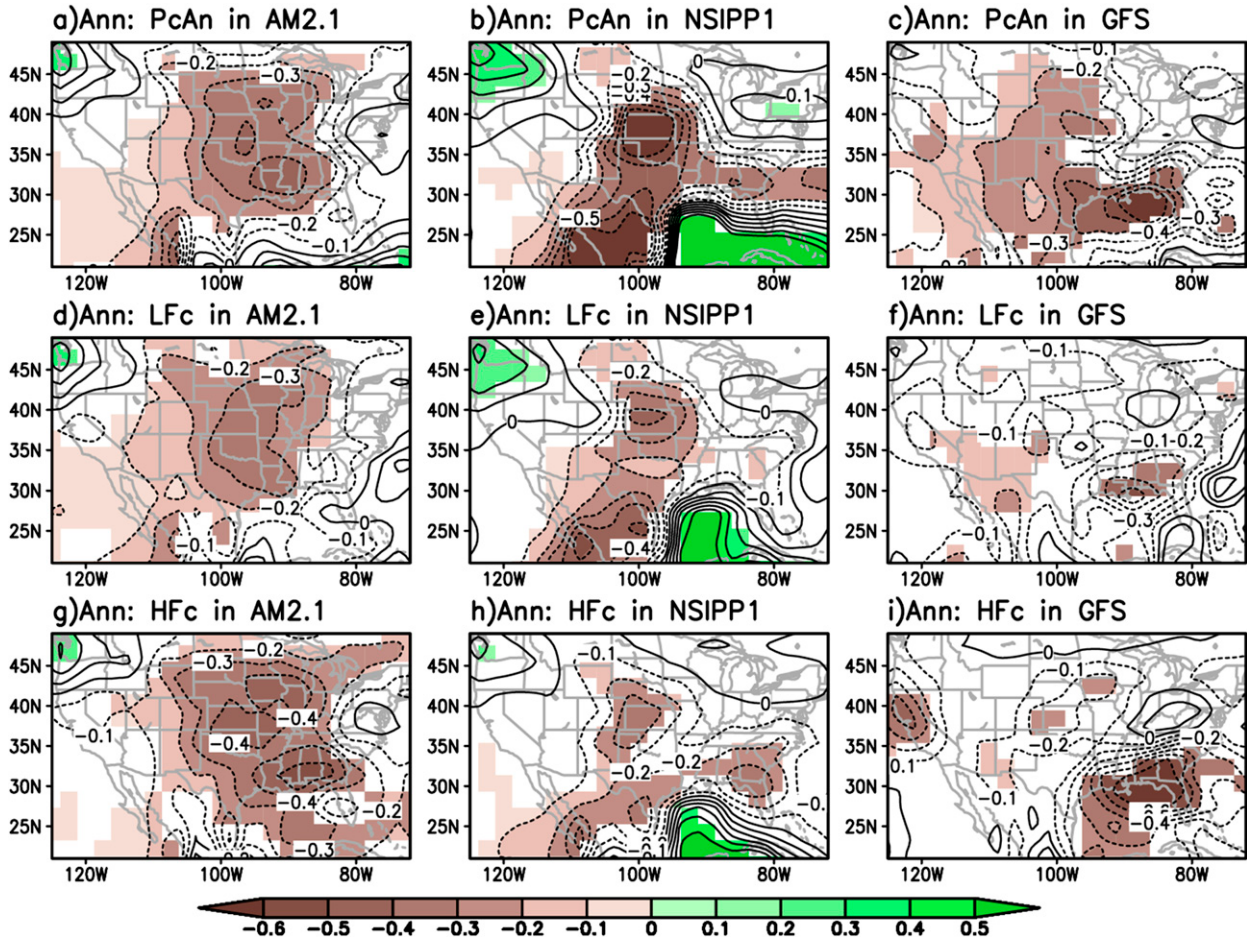


FIG. 3. Models-simulated annual mean precipitation responses (mm day^{-1}) to the (top) PcaN, (middle) LFc, and (bottom) HFc SST anomaly patterns in (left) AM2.1, (center) NSIPP1, and (right) GFS. The anomalies are computed with respect to the control simulated (PnAn) annual mean response with prescribed global climatological SSTs only. Shading indicates confidence at 90%.

annual mean drought response (Figs. 3c,f,i) is also largest in the PcaN simulation and for the Great Plains and much of the U.S. Southwest. For the LFc and HFc forced simulations, the amplitude of the drought response is considerably reduced in the Great Plains, though the HFc simulation retains large amplitude in the U.S. Southeast.

Figure 4 shows the distribution of the annual mean precipitation response in three AGCMs for the three forcing patterns shown in Fig. 1. The response in this case is measured as the difference between gridpoint values of annual mean experimental precipitation and the time mean precipitation response of the control (full field SST climatology only) simulation. The results are presented by subregion as described in Fig. 2 and the data are grouped by model within each subregion. The shading of the interquartile range (IQR) identifies the simulation (dark green for PcaN, medium green for LFc, and light green for HFc), and the line (circle) in the center of the box represents the median (mean).

In the northwestern United States (Fig. 4a), the mean precipitation responses are distributed near zero and are slightly negative, with the exception of the NSIPP1 PcaN and LFc simulations, where the median values are slightly positive. This is consistent with the larger area of significant positive precipitation anomalies near the coast in Figs. 3b and 3e. For the AM2.1 model, the median precipitation responses are centered slightly negative, with dry conditions in the eastern portion of the NW region and a smaller region of positive values in the Pacific NW. The AM2.1 responses are consistent across all forcing patterns, with slightly larger negative amplitude in the HFc simulation. In the NSIPP1 model, there is a noticeable positive shift from the HFc simulation to the PcaN and LFc simulations. This result suggests increased sensitivity in the NSIPP1 model to forcing from the middle latitudes or possibly the eastern subtropical Pacific, as the HFc forcing pattern has minimal amplitude there with respect to the LFc and PcaN patterns. The GFS response in the

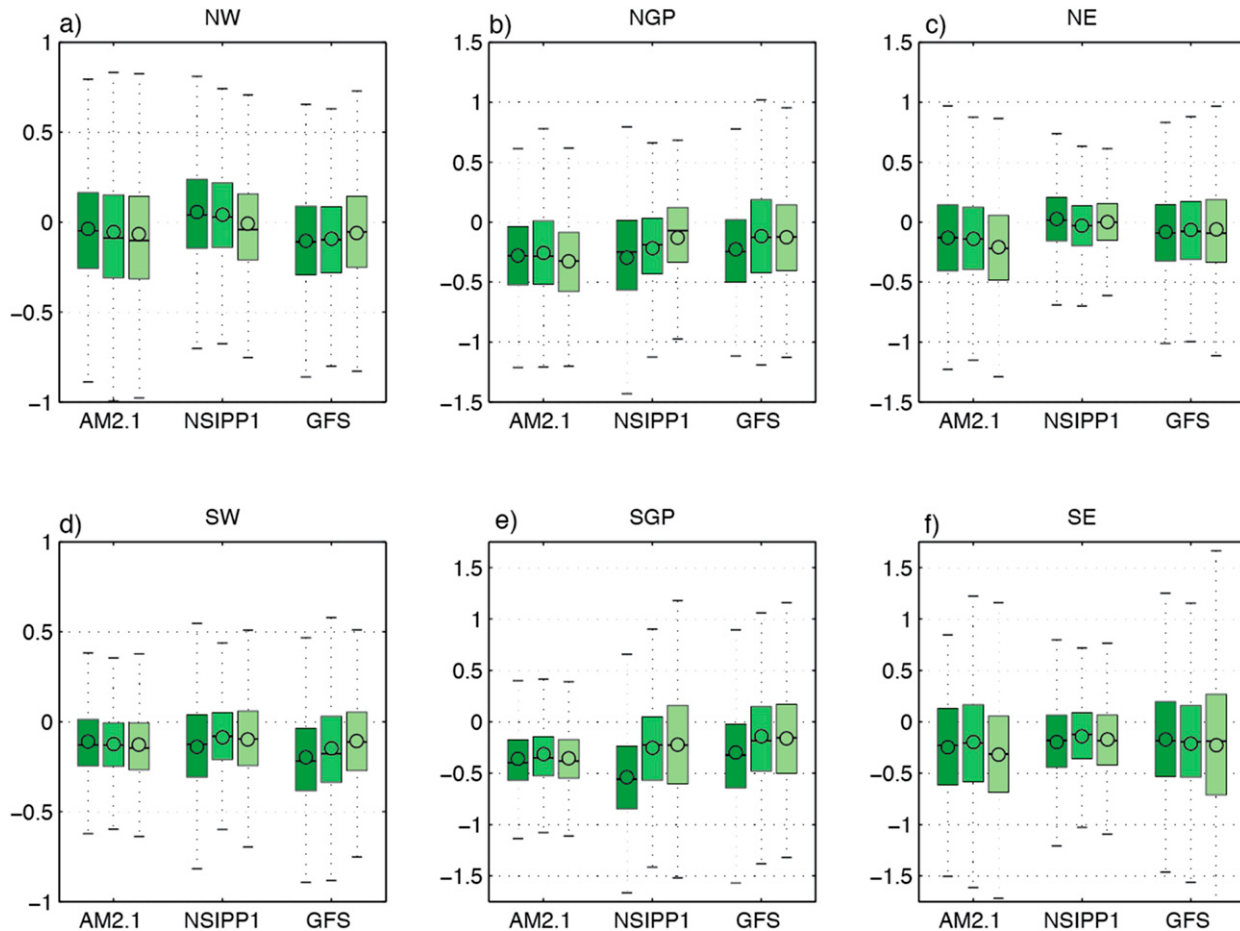


FIG. 4. Box-and-whisker plot of the simulated annual mean model precipitation difference (mm day^{-1}) from control (PcAn) simulation for the regions shown in Fig. 3 and labeled at top. PcAn (dark green), LFc (medium green), and HFc (light green) box plots are shown from left to right and are grouped by model within each panel (labeled at bottom). The shading in the boxes covers the IQR of precipitation with median (mean) identified by central horizontal line (circle), whiskers extend to $Q_1 - 1.5 \times \text{IQR}$ and $Q_3 + 1.5 \times \text{IQR}$ or 2.698σ .

NW is slightly negative for all forcing patterns, with more drying in the PcAn simulation. In the U.S. Southwest, the drought response is robust across all models and forcing simulations (Fig. 4d). The spread is generally small across all models here, as expected for such an arid region, though it is slightly larger in NSIPP1 and GFS models. There is also a stronger drought response in the NSIPP1 and GFS PcAn simulations with respect to HFc and LFc than is seen in AM2.1, where HFc is slightly drier.

In the northern Great Plains region (NGP), the amplitude of the annual mean precipitation response is larger than in the U.S. Southwest for all models (Fig. 4b; note change of scale). There is a robust drought response for the PcAn forcing pattern over the northern Great Plains region for all models, though the HFc simulation is slightly stronger in the AM2.1 model. The NSIPP1 median drought response weakens from the PcAn simulation to the LFc and the HFc simulations, respectively, again suggesting a larger role for the

extratropical component of the forcing. For the GFS model, the drought response in the PcAn simulation is largest, while the HFc and LFc drought responses are weaker and comparable to each other.

In the southern Great Plains (SGP), the NSIPP1 and GFS models show much more variability in the precipitation response than the AM2.1 model, and the PcAn forced simulations again showed the largest amplitude drying. The AM2.1 response to the differing forcing patterns is again in strong agreement. For the NSIPP1 model, the PcAn simulation is stronger and well separated from the LFc and HFc simulations, though there is no clear separation between HFc and LFc as in the NGP region. The strong agreement between the AM2.1 simulations suggests that while the model is sensitive to the SST forcing, there is less sensitivity to the differences in the details in forcing patterns from the midlatitudes to the equator for this region. The distribution of the GFS annual precipitation response in the SGP is similar to

that in the NGP, with a strong drought response in the P_cA_n simulation and a weaker response in the HFc and LFc simulations.

In the northeastern United States (NE; Fig. 4c), the median precipitation values are negative in all of the AM2.1 simulations, with slightly stronger drying in the HFc simulation, consistent with the stronger negative precipitation anomalies seen in the Midwest in Fig. 3g. For the NSIPP1 model, the median precipitation response is centered near zero, with dry conditions in the western portion of the NE region and a smaller region of positive values to the east (see Fig. 3b). The spread is also reduced in the NSIPP1 simulation with respect to the other AGCMs. The mean GFS precipitation response in the NE region is slightly negative and consistent across all forcing patterns. It is clear from the results shown in Fig. 3 that the inclusion of the Midwest into the NE subregion has significant implications for the results in Fig. 4c. The drought signal in the Midwest (western NE subregion) is strong and significant in the P_cA_n simulation for all of the models, while the amplitude and significance of the response is reduced in the eastern half of the NE subregion. Further analysis of the northeast region east of the great lakes shows a shift in the distribution toward zero (not shown). The lack of significant values in the eastern portion of the subregion suggests a reduced role for Pacific SSTs here (Schubert et al. 2009).

In the U.S. Southeast (SE; Fig. 4f), model responses again shift to negative, and there is a marked increase in spread for the AM2.1 and GFS simulations. For the AM2.1 simulations, the HFc simulation has the largest mean drought response, though the spread is reduced in the P_cA_n simulation. The median NSIPP1 responses show good agreement between the forcing patterns, with slightly smaller amplitude (negative) median values in the LFc simulation and less spread than the other AGCMs. The GFS simulations show similar median amplitude responses for all forcing patterns, though the spread is larger in the HFc forcing simulation.

b. Seasonality of Great Plains precipitation response

Figure 5 shows the annual mean and seasonal progression of model precipitation climatology (dark blue bars, from P_nA_n control simulation) and precipitation anomalies (colored circles) over the northern (Figs. 5a–c) and southern (Figs. 5d–f) Great Plains in the idealized AM2.1, NSIPP1, and GFS simulations. Also shown in Figs. 5a–f is the annual mean and monthly climatology of precipitation for the northern and southern Great Plains from observations (light blue bars). We first consider the annual mean precipitation response (labeled MN; first column) of the models over the northern and southern Great Plains. For both regions, the AM2.1

and NSIPP1 AGCMs underrepresent the annual mean rainfall (dark blue bars), particularly the AM2.1 model in the SGP, while there is too much precipitation in the GFS model. In agreement with the results shown in Figs. 4b and 4e, the annual mean precipitation anomalies (solid colored circles) for the AM2.1 simulations are nearly equivalent, though the HFc and P_cA_n have slightly larger amplitude. For the NSIPP1 and GFS AGCMs, the amplitude of the precipitation response in the P_cA_n simulation is clearly larger than the HFc or the LFc simulations in both GP subregions.

The connected colored circles in the remaining columns of Figs. 5a–f describe the seasonal precipitation response to P_cA_n, LFc, and HFc forcing patterns for the three AGCMs. Solid circles identify significant values. For AM2.1 (Figs. 5a,d), significant dry conditions are present in the northern Great Plains from March through August, with peak drought conditions in May and a gradual return to near-normal conditions for the autumn and winter months. In the southern Great Plains, significant dry conditions are present from January to July in each AM2.1 simulation, with peak drought conditions in May and a rapid shift to near-normal conditions in the summer season when the model precipitation climatology is small with respect to observed estimates. As with the annual mean, the monthly deviations for the three forcing patterns are coherent in amplitude over time.

Figures 5b and 5e show the monthly deviations of precipitation in the NSIPP1 simulations. There is little significant drought response for the northern Great Plains in the winter season of the NSIPP1 simulations. Significant dry conditions are present in the northern Great Plains from April to October in each simulation, with the exception of the HFc response in August and September (Fig. 5b), and the spread between the simulations is largest in the summer months. The peak drought conditions occur in July in all NSIPP1 simulations in contrast to peak drought in May in AM2.1. In the southern Great Plains, significant dry conditions among the three simulations are less coherent over the year. Drought conditions are simulated for all but one month in the P_cA_n simulation (Fig. 5e), with peaks in winter and summer months. During the P_cA_n and LFc peak drought month of July, there is no significant drought in the HFc simulation, and there is no significant drought in December in the LFc simulation when HFc and P_cA_n show a peak. The large annual mean response for the P_cA_n simulation is clearly influenced by the presence of both strong summer and winter responses.

Figures 5c and 5f show the monthly climatology and precipitation anomalies in the northern and southern Great Plains subregions for the GFS simulations. For the northern Great Plains, the climatological precipitation in

Mean/Monthly Precipitation over Southern/Northern Great Plains

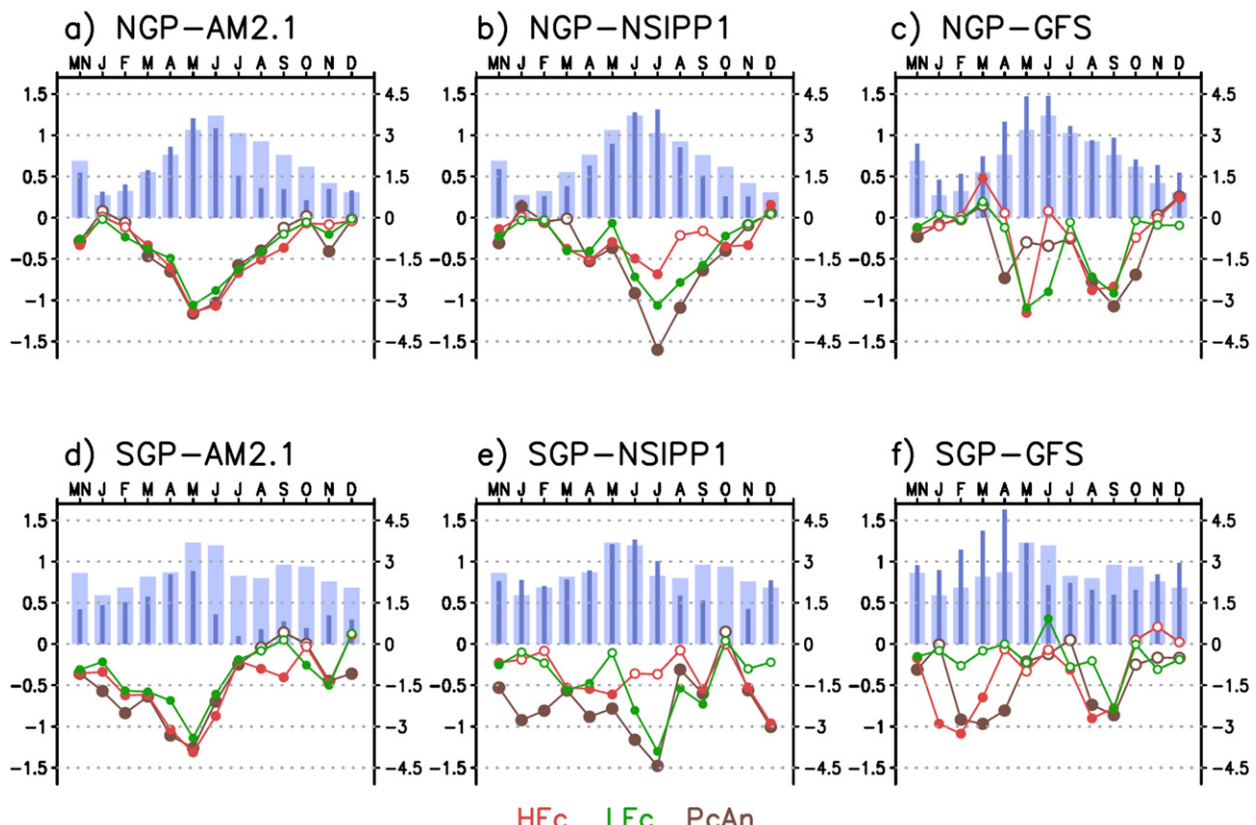


FIG. 5. Annual mean (labeled MN in the top far left of each panel) and monthly precipitation climatology and simulated precipitation response with respect to control (PnAn) averaged over (a)–(c) the northern Great Plains and (d)–(f) the southern Great Plains. Model annual mean and monthly mean climatology is shown with dark blue bars for each case; and observed annual mean and monthly climatology are shown with light blue bars (right-hand side y axis; mm month⁻¹). Annual mean and seasonal response of HFc (red), LFc (green), and PcAn (brown) compared to climatology control run. Solid circles indicate confidence at 90% (left-hand side y axis; mm day⁻¹).

the GFS is larger than the observed estimates (dark blue bars), though the observed seasonality is well simulated. The seasonal cycle of drought in the GFS in the northern Great Plains is less coherent than that of AM2.1 and NSIPP1, with no significant drought response from November through March and a coherent drought signal in all forcing simulations for August and September only. There is also a May peak in the LFc and HFc simulations. In the southern Great Plains, the LFc simulation only simulates significant drought in September. The HFc and PcAn simulations are more coherent and simulate significant drought conditions from February to March and from August to September. In a recent study by Koster et al. (2006), the Great Plains was identified as one of several “hot spots” on the globe for the importance of land-atmosphere coupling in accurately simulating summer season precipitation. The authors found that the GFS model had weak land-atmosphere coupling strength in the

Great Plains when compared to the NSIPP1 and AM2.1 models. Our interpretation of the results is that this reduced coupling is likely a strong influence on the observed lack of coherence in the GFS summer season drought response.

c. Spring and summer AGCM precipitation response

Figures 6a–i shows composite averages of the spring [March–May (MAM)] season precipitation response for three AGCMs to the three forcing patterns shown in Fig. 1. The MAM response is robust for all AGCMs for the PcAn forcing pattern. For AM2.1, the MAM drought response to all three forcing patterns is widespread, with larger amplitude in the Great Plains and southeastern United States in the HFc and PcAn simulations (Figs. 6a,d,g). In the summer season [June–August (JJA); Figs. 7a,d,g], the AM2.1 drought propagates to the U.S. Northeast for all forcing patterns, consistent with the

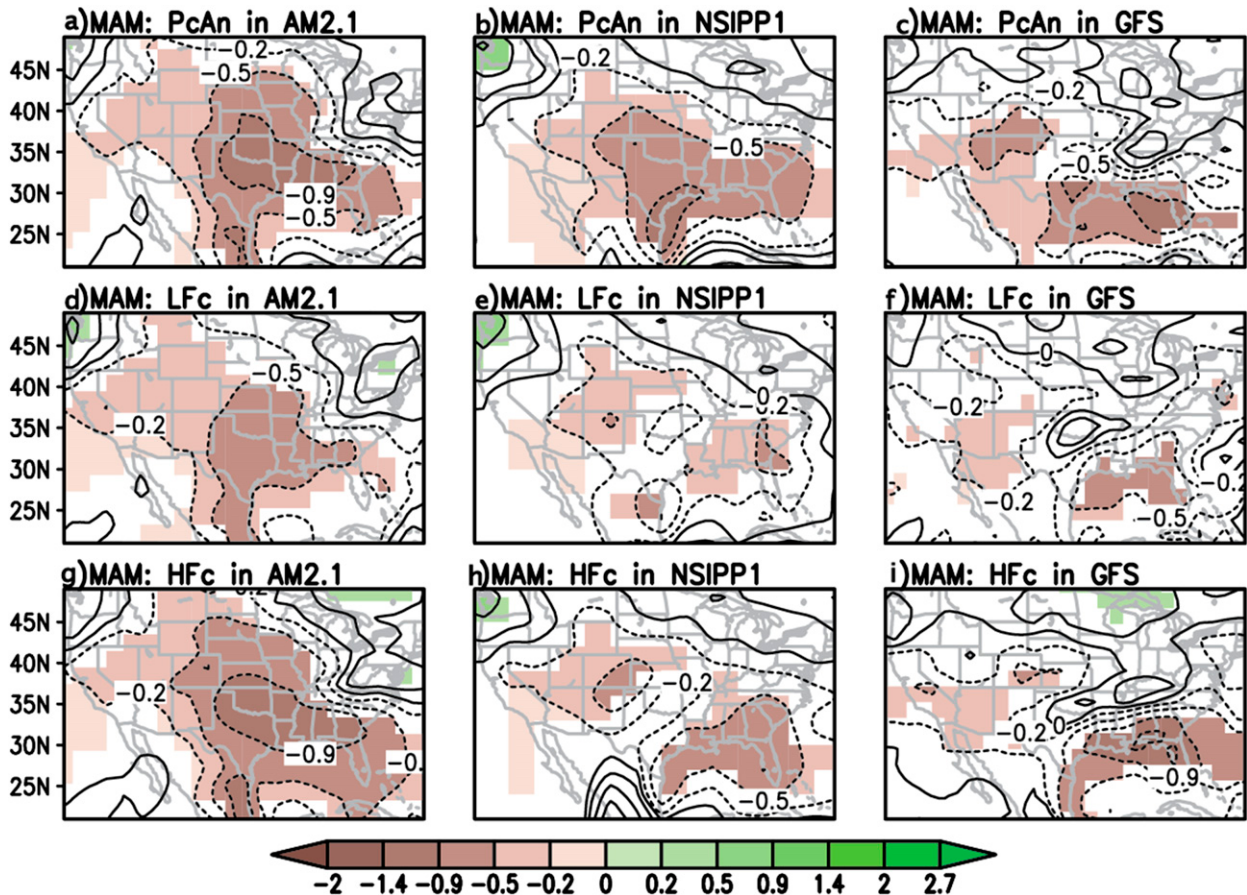


FIG. 6. Simulated seasonally averaged precipitation response (mm day^{-1}) during MAM season with respect to control (PnAn) simulations. The MAM responses in AM2.1 to (a) PcAn, (d) LFc, and (g) HFc. The MAM responses in NSIPP1 to (b) PcAn, (e) LFc, and (h) HFc. The MAM responses in GFS to (c) PcAn, (f) LFc, and (i) HFc. The contours are the seasonal mean, and 90% confident values of the seasonal mean are shaded.

reduction in the southern Great Plains drought seen in Fig. 5d.

Figures 6b, 6e, and 6h show the spatial characteristics of the spring season drought response in the NSIPP1 AGCM. During the spring season, the spatial characteristics of the NSIPP1 precipitation response are in good general agreement with the spring response of the AM2.1 simulations, though with reduced amplitude and significance in LFc and HFc simulations in the central United States. This leaves two centers of action in the Rocky Mountain states and throughout the southeastern United States. In the summer season, all of the NSIPP1 simulations shift to two centers of action over Mexico and the central Great Plains (Figs. 7b,e,h). The reduced amplitude of the SGP HFc simulated JJA drought response seen in Fig. 5e is evident for the summer months, as is the amplified response of the PcAn simulation. There is also a large positive precipitation anomaly over the Gulf of Mexico in the summer months associated

with a low-level cyclone (Wang et al. 2010), with the largest amplitude in the PcAn simulation.

Figures 6c, 6f, and 6i show the spatial characteristics of the spring season drought response in the GFS AGCM. During the spring season, the spatial characteristics of the composite GFS precipitation response have reduced amplitude and significance in the northern Great Plains subregion in the PcAn simulation and little significant drying in either subregion in the LFc or HFc simulations. This is likely because of the small-amplitude (or positive) response in the region during March and April (Fig. 5c) in the composite average. In the southern Great Plains, the PcAn and HFc simulations have significant drying in Kansas, western Colorado, and Texas during the spring. During the summer season (Figs. 7c,f,i), when internal atmospheric variability is largest, there is little significant drought in any of the GFS simulations.

Differences in the precipitation responses can be better understood by viewing the composite average

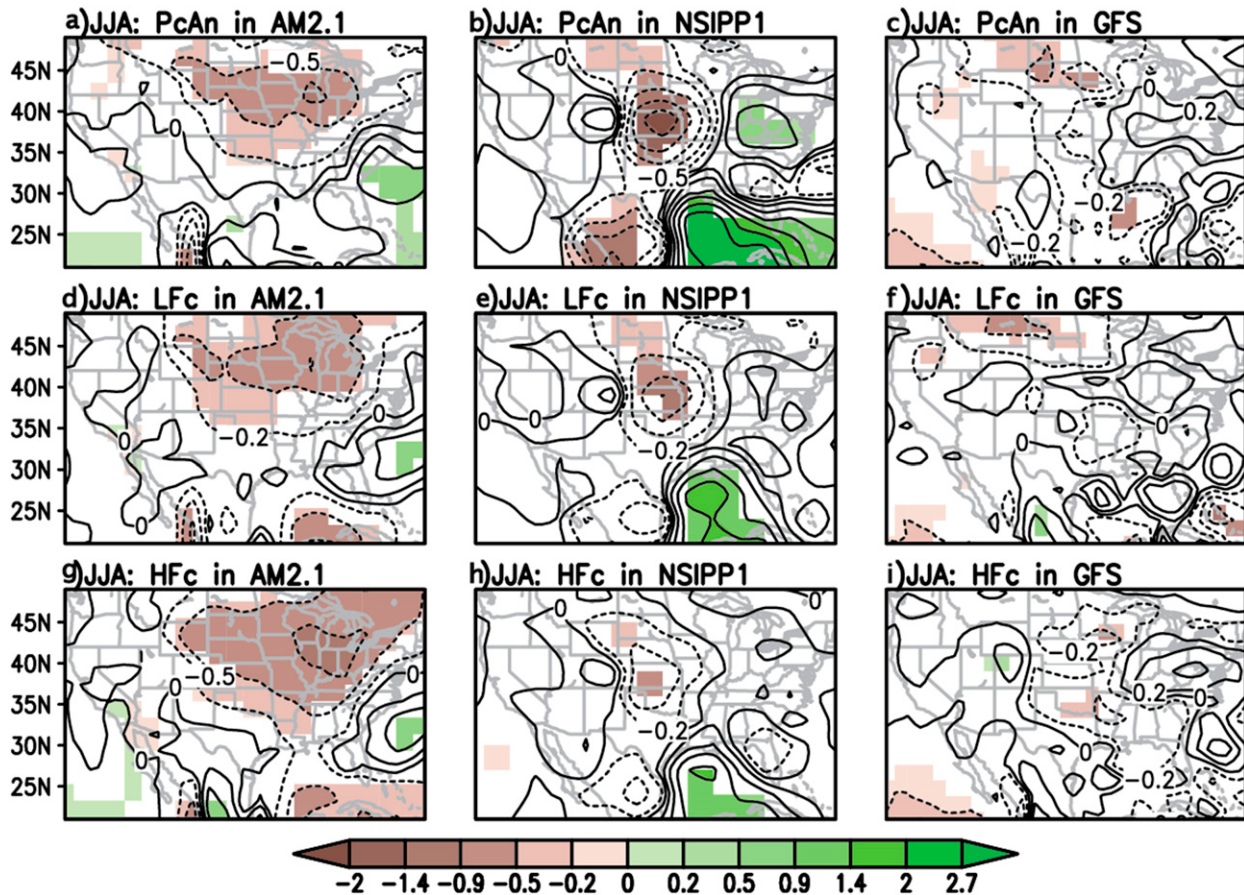


FIG. 7. As in Fig. 6, but for the summer (JJA).

200-hPa geopotential height (Z200) response for the AGCM simulations during spring and summer seasons (Figs. 8a–h). Schubert et al. (2009) show the Z200 pattern annual mean response of the PcAn simulations, with positive heights extending across the Pacific in both hemispheres, consistent with the results of Hoerling and Kumar (2003) and Seager et al. (2003, 2005). The spring season Z200 composite patterns are similar in structure for all SST forcing patterns in the three models; thus, only the PcAn response is shown for MAM (Figs. 8a,e,i). The spring Z200 patterns are generally similar between the NSIPP1 and AM2.1 models over the southern continental United States, with positive height anomalies centered over the western United States extending east through the Great Plains subregions. The strength and structure of this ridge of high pressure has been shown to be directly coupled to reduced precipitation in the underlying region and is associated with a poleward shift in the subtropical jets, with anomalous warming and descent (not shown).

Figures 8b–d shows the JJA Z200 composite anomalies for the PcAn, LFc, and HFc simulations of the

AM2.1 AGCM. The AM2.1 AGCM simulates a similar height response pattern for all forcing patterns, characterized by positive heights in the eastern subtropical Pacific and in the near-northern region of Canada and negative heights in the Gulf of Alaska and off the coast of the mid-Atlantic states (spatial correlations for PcAn and LFc, $r = 0.90$; PcAn and HFc, $r = 0.85$; and HFc and LFc, $r = 0.90$). The positive heights in the near-northern region of Canada are consistent with the northeast movement of the drought seen in Fig. 7. The NSIPP1 simulates positive heights over much of the northern continental United States, with negative heights over the southern states and Mexico. The height response is strongest for the PcAn forcing pattern and becomes progressively weaker in the LFc and HFc simulations. This change is consistent with the precipitation composites in Fig. 6 and the seasonal drought response in the Great Plains shown in Fig. 5. For the NSIPP1 simulations, the Z200 response is not as well correlated between forcing patterns as in AM2.1 (PcAn and LFc, $r = 0.84$; PcAn and HFc, $r = 0.82$; and HFc and LFc, $r = 0.67$), though the differences in the spatial correlations are more in line with the differences

Z200 Response

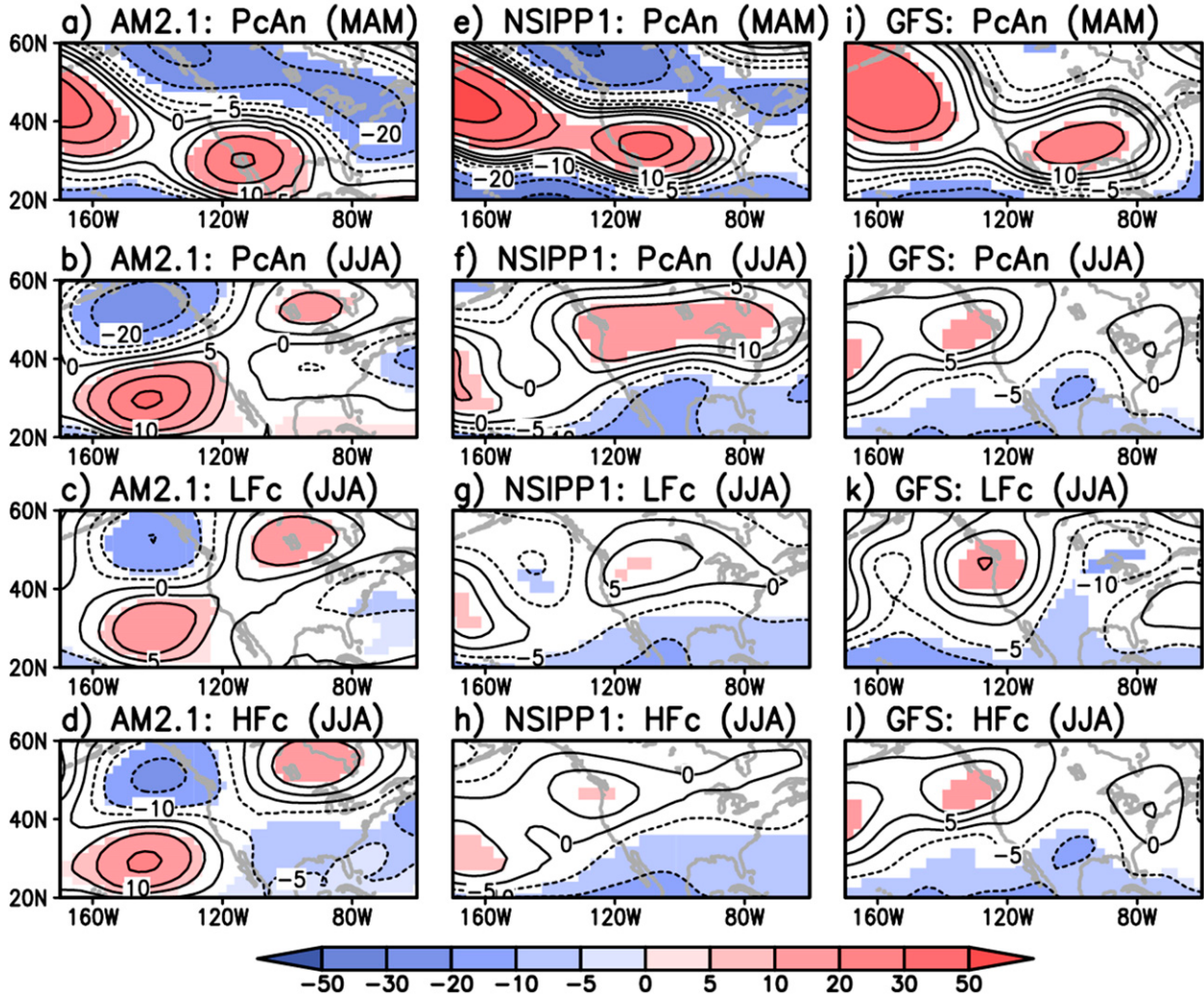


FIG. 8. Simulated 200-hPa geopotential height difference from control simulation (PnAn). AM2.1 (a) MAM PcAn, (b) JJA PcAn, (c) JJA LFc, and (d) JJA HFc response. NSIPP1 (e) MAM PcAn, (f) JJA PcAn, (g) JJA LFc, and (h) JJA HFc response. GFS (i) MAM PcAn, (j) JJA PcAn, (k) JJA LFc, and (l) JJA HFc response. The contour intervals are 5 m, and shading denotes 90% confidence.

in the spatial correlations of the SST forcing patterns. We note that Wang et al. (2010) attribute more of the simulated summer season Great Plains drought signal to a reduction in the low-level jet associated with the low-level cyclone in the Gulf of Mexico than with the teleconnection patterns shown here. In the GFS simulation, the ridge is shifted further to the east during spring and covers most of the contiguous United States. During JJA, the ridge that covers most of the contiguous United States during the spring is absent, with positive anomalies confined to the Pacific Northwest (Figs. 8j–l). For the GFS simulations, the coherence between the Z200 responses is further reduced (spatial correlations for PcAn and LFc, $r = 0.80$; PcAn and HFc, $r = 0.61$; and HFc and LFc, $r = 0.63$).

In Fig. 9, we examine the signal-to-noise ratio of the Z200 response to better understand the degree to which internal variability obscures the summer season precipitation signal forced by the SST anomalies. Following the procedure in Schubert et al. (2009), we show the quantity

$$R = \left(\frac{\bar{x} - \bar{y}}{s_{xy}} \right),$$

where the x and y are seasonal averages at each grid point from the experiments and the control simulations, respectively, the overbar denotes the 50-yr mean (35-yr mean for the GFS model), and $S_{xy}^2 = (S_x^2 + S_y^2)/2$, where S_x^2 and S_y^2 are the variance estimates of x and y ,

Z200 : R

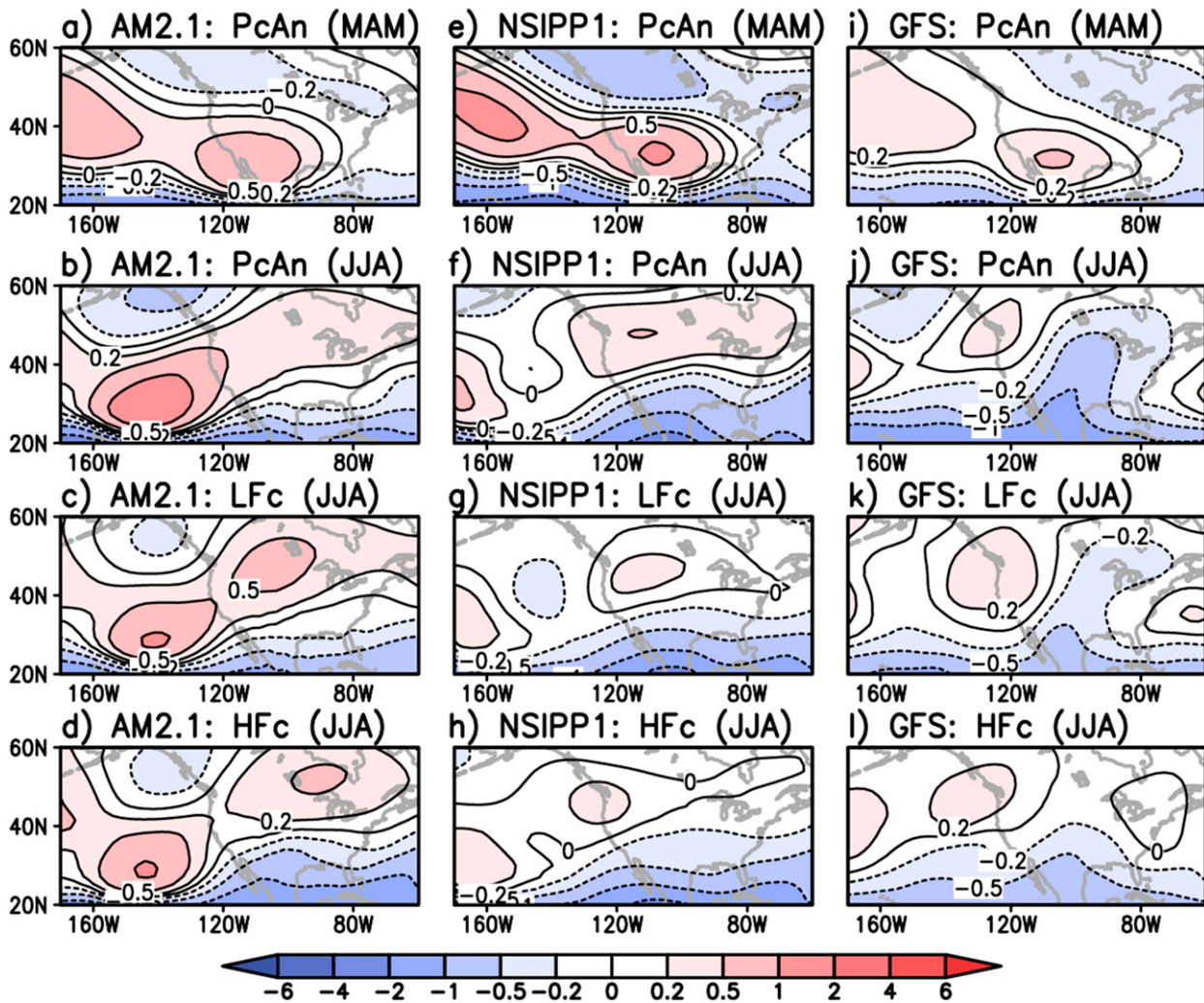


FIG. 9. Signal-to-noise ratio (R), of 200-hPa geopotential height response during MAM and JJA seasons. AM2.1 (a) MAM PcAn, (b) JJA PcAn, (c) JJA LFc, and (d) JJA HFc. NSIPP1 (e) MAM PcAn, (f) JJA PcAn, (g) JJA LFc, and (h) JJA HFc. GFS (i) MAM PcAn, (j) JJA PcAn, (k) JJA LFc, and (l) JJA HFc. The contour intervals are denoted by the color bar, and shading denotes 90% confidence.

respectively. The difference in means in the numerator represents the signal, and R measures the size of the signal in units of standard deviation. Figures 9a, 9e, and 9i show a strong signal in all models for the spring season, though the GFS model has smaller amplitude. Figures 9b–d show that for the AM2.1 simulations, the signal remains quite strong into the summer months in all of the forcing simulations; while the GFS summer response indicates a much more dominant role for internal atmospheric variability in the summer months. The NSIPP1 summer response (Figs. 9f–h) also illustrates a greater influence of internal variability in the model during the summer months. This result is consistent with Wang et al. (2010), who showed that the largest

divergence in simulated precipitation and atmospheric circulation responses of the DWG baseline simulations occurred during warm seasons. However, the stronger summertime signal to noise seen in Fig. 9f is consistent with the hypothesis that constructive interference between the large middle latitude (Fig. 9g) and equatorial (Fig. 9h) forcing is occurring in the PcAn simulation in the NSIPP1 model, resulting in the larger drought signal in Fig. 7b.

d. NSIPP1 spring and summer teleconnection patterns

The results thus far indicate that the NSIPP1 AGCM shows a regional sensitivity to the differing forcing

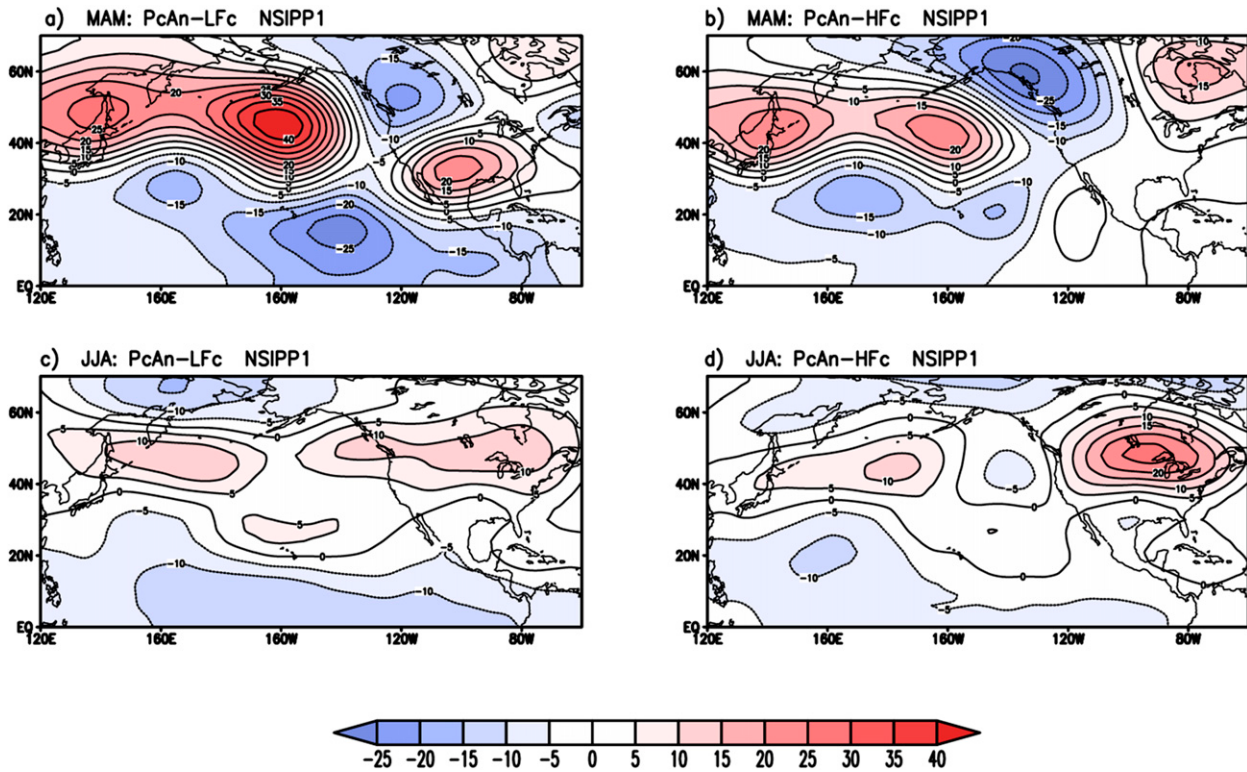


FIG. 10. Simulated 200-hPa geopotential height response in the NSIPP1 AGCM. (a) Pcan-LFc for MAM; (b) Pcan-HFc for MAM; (c) LFc for JJA; and (d) Pcan-HFc for JJA. The contour intervals are 5 m.

patterns, with a larger-amplitude response in the Pacific Northwest and northern Great Plains in the Pcan and LFc simulations compared to the HFc simulation, while the response to the Pcan and HFc simulations was larger in the U.S. Southeast compared to the LFc. To elucidate the possible mechanisms for this sensitivity, we examine the differences in the atmospheric response of the HFc and LFc simulations with respect to the Pcan simulation. Figure 10 shows the difference between the Z200 responses of the Pcan simulation and the LFc and HFc simulations during the spring (Figs. 10a,b) and summer (Figs. 10c,d) seasons in the NSIPP1 AGCM. The large difference (0.6°C , not shown) in the eastern equatorial SSTA amplitude between Pcan and LFc is clear during the spring (Fig. 10a), with a strong negative PNA wave response. The SST difference between the Pcan forcing pattern and the HFc pattern is characterized by stronger positive (negative) amplitude in the central (eastern) extratropical regions of 0.3°C and reduced amplitude throughout the equatorial Pacific (not shown). The difference in the MAM response seen in Fig. 10b is clearly strongest in the northern United States and Canada and is consistent with the results of Latif and Barnett (1994), who forced their AGCM with a pattern

of SSTs similar to Pcan, where anomalies south of 25°N were neglected. However, we note that the response is also consistent with the results of Barsugli and Sardeshmukh (2002), who forced a GCM with anomaly patches throughout the tropical Pacific (12.5°S – 12.5°N). While we do not dispute the sensitivity of the northwestern United States and northern Great Plains sub-regions to SSTs in the west Pacific (e.g., Yu et al. 2012), we emphasize that the amplitude of the equatorial forcing in the Niño-4 region is weaker in the LFc pattern than in the Pcan and HFc patterns. Thus, it is our contention that the precipitation response in these regions is the result of the extratropical component of the forcing. This result is also consistent with the results of Schubert et al. (2004a), who ran fixed SST experiments with NSIPP1 using a similar pattern to Pcan in full field and tropics-only ($\pm 20^{\circ}$ latitude) simulations. The authors showed that the simulation that included the extratropical component of the SST pattern had a larger-amplitude drought response in the Great Plains region. For the summer season responses (Figs. 10c,d), the amplitude of the Z200 response is significantly reduced, though the influence of the midlatitudes is still apparent in Fig. 10d, while a zonally symmetric response is more apparent for a stronger equatorial signal (Fig. 10c).

4. Summary and discussion

Idealized atmospheric model simulations run as a part of the U.S. CLIVAR Drought Working Group were analyzed to determine the impact of three Pacific SST anomaly patterns on the contiguous United States. The patterns included a Pacific (PcAn) pattern that was incorporated in the baseline experiments of the DWG with large amplitude along the equator and in the midlatitudes, a low-frequency cold pattern with reduced amplitude along the equator and large amplitude in the middle latitudes, and a high-frequency cold pattern with large amplitude on the equator and little amplitude in the middle latitudes or western tropical Pacific. Three models were analyzed.

Overall, there is agreement with previous results using the DWG model data, as all of the models simulated drought conditions over large portions of the contiguous United States for the La Niña-like PcAn SST forcing pattern (Schubert et al. 2009). For the HFc and LFc forced simulations, the AGCMs also consistently simulated warm (not shown), dry conditions over large regions of the contiguous United States (particularly the Great Plains region) in the annual mean. Consistent with observations, the AM2.1 and NSIPP1 models also simulated significant increases in annual mean precipitation in the Pacific Northwest.

Building on previous results of the DWG, the current study finds differing levels of sensitivity to regional differences in prescribed Pacific SST forcing patterns with respect to internal atmospheric variability in the three AGCMs. The coherence of the AM2.1 responses for all forcing patterns and across all seasons suggests the model is overpredicting the strength of the tropical SST signal. Internal atmospheric variability and land-atmosphere interactions clearly influence the GFS model response, though the shorter simulations also play a role in the reduced significance of the results presented. The SST forced response in the NSIPP1 AGCM is a function of the relative amplitude of the SST forcing in the tropics and middle latitudes, with detectable constructive interference between the two signals, similar to that seen between ocean basins (McCabe et al. 2004; Schubert et al. 2009). The constructive interference is also evident in the GFS PcAn simulation in the U.S. Southwest and Great Plains regions. Further, the current study points to a more significant role for the extratropical component of the SST in forcing the precipitation response; particularly over the western United States and northern Great Plains, via distinctly different teleconnections. This result suggests that the tropical mechanisms described in previous studies (e.g., Barsugli and Sardeshmukh 2002; Seager et al. 2003; Hoerling and Kumar 2003) may work in combination with

the extratropics to affect North American hydroclimate. The seasonal response in the Great Plains region also points to a more complex picture for the SST-hydroclimate relationship and highlights the important roles that internal atmospheric variability and soil moisture feedback play in modulating the SST forced signal. The seasonality of the drought response in the three AGCMs varied considerably for the Great Plains region, and it is unclear to what degree the simulated seasonal cycle of precipitation plays a role in determining the seasonality and peak period of the drought response in conjunction with the internal atmospheric variability and soil moisture feedback.

The coherent response of the AM2.1 AGCM with respect to NSIPP1 raises the following question: "How much of the response is just attached to the tropical SST forcing?" Newman et al. (2003) argued that the PDO (analogous to our LFc pattern) was an artifact of interannual (ENSO) variability in the equatorial Pacific. The authors were able to predict much of the observed PDO behavior using a very simple predictive model and an observed ENSO index. The authors argued that SST anomalies in the extratropics are forced by ENSO via an atmospheric bridge and argued that the observed multiyear persistence of the SSTAs in the extratropics are a result of decoupling in the summer season deep ocean mixed layer and subsequent "reemergence" of the anomalies in the winter season (Alexander et al. 1999, 2002).

Whether the observed pattern of decadal variability in the Pacific is an independent mode of variability operating on decadal time scales or exists as an integrator of ENSO is beyond the scope of this study. If the PDO is simply an integrator of ENSO, then perhaps the persistent drought response seen over the past 16 years is similarly an integrated effect of the more numerous La Niña events manifested in the Great Plains land surface moisture budget. Alternatively, the persistence of the middle latitude SST anomalies across years via the reemergence mechanism may play an important role in preconditioning the western United States and Great Plains regions via teleconnections, as indicated in Fig. 10b, independent of the equatorial forcing.

The DWG methodology does have several shortcomings. The patterns of variability used in the simulations are derived from statistical analyses and are prescribed with fixed amplitude and spatial structure that cannot capture the broad spectrum of patterns seen in the observations. The time-independent forcing also misrepresents the time evolution of the phenomena they represent, particularly in the equatorial Pacific. Further, the persistent forcing experiments underplay the role of natural atmospheric variability in causing persistent drought (Hoerling et al. 2013).

We suggest, however, that the utility of the DWG simulations lies in the simplicity of their formulation. The numerous baseline experiments (and additional runs like the HFc and LFc) need to be computationally efficient and effectively isolate the response to the mode of variability in question. The experimental design of the U.S. CLIVAR Drought Working Group provides a valuable resource for model evaluation and mechanistic studies of the Pacific Ocean's influence on North American hydroclimate. While current prediction efforts, such as the North American Multimodel Ensemble system (Kirtman et al. 2014), capitalize on the increased skill found in multimodel means to bring improved forecasts to water resource managers and decision makers, there is a demand for simple mechanistic studies like the one performed here that focus on processes and potential sources of predictability.

In light of the results presented, it is certainly reasonable that the amplitude of the Pacific (PcAn) pattern dominated the drought response in the earlier works by the U.S. CLIVAR Drought Working Group (Schubert et al. 2009), when compared to the multidecadal Atlantic and warming trend patterns. In our subset, each of the models showed a large response in the presence of persistent large-amplitude equatorial and midlatitude SSTAs. While the large equatorial component of the PcAn forcing may not be appropriate for comparison with the decadal- and century-scale Atlantic multidecadal oscillation (AMO) and global trend pattern, it is critical in the context of understanding the observed variability of the Pacific. The PcAn pattern can be seen as a “worst case” scenario for drought that is all the more relevant considering the recent occurrence of multiyear La Niña events (1998–2001, 2007–09, and 2010–12). The amplified response to the combined PcAn pattern seen in the NSIPP1 AGCM suggests that the severity of several recent droughts, particularly in the U.S. Southwest and Great Plains, is likely influenced by the combined cold decadal pattern that has prevailed since the late 1990s (Burgman et al. 2008a; Clement et al. 2009) and the large number of individual La Niña events.

Coupled model simulations with increasing levels of well-mixed greenhouse gases indicate that warming surface temperatures may lead to a weaker vertical overturning circulation and a poleward shift in the storm tracks, leading to more arid conditions for the United States (Yin 2005; Meehl et al. 2005; Seager et al. 2007). Concurrently, several recent studies indicate that natural variability of SSTs on interannual-to-multidecadal time scales is still playing a significant role (Burgman et al. 2008a; McGregor et al. 2014). For a region like the Great Plains that is sensitive to seasonality and extratropical forcing, a better understanding of the relative

influence of regional Pacific SST forcing on multiyear droughts will become even more important for decision makers as the hydrologic base state of the United States changes over the coming century.

Acknowledgments. We acknowledge the U.S. CLIVAR Drought Working Group and the associated modeling agencies for producing and making available their model output. We thank the anonymous reviewers for improving this manuscript with their insightful suggestions. This work is supported by the NOAA climate program office (Grant NA10OAR4310203).

REFERENCES

- Adler, R. F., and Coauthors, 2003: The Version-2 Global Precipitation Climatology Project (GPCP) Monthly Precipitation Analysis (1979–present). *J. Hydrometeor.*, **4**, 1147–1167, doi:10.1175/1525-7541(2003)004<1147:TVGCP>2.0.CO;2.
- Alexander, M. A., C. Deser, and M. S. Timlin, 1999: The reemergence of SST anomalies in the North Pacific Ocean. *J. Climate*, **12**, 2419–2431, doi:10.1175/1520-0442(1999)012<2419:TROSAT>2.0.CO;2.
- , I. Bladé, M. Newman, J. R. Lanzante, N.-C. Lau, and J. D. Scott, 2002: The atmospheric bridge: The influence of ENSO teleconnections on air-sea interaction over the global oceans. *J. Climate*, **15**, 2205–2231, doi:10.1175/1520-0442(2002)015<2205:TABTIO>2.0.CO;2.
- Bacmeister, J., P. J. Pegion, S. D. Schubert, and M. J. Suarez, 2000: Atlas of seasonal means simulated by the NSIPP 1 atmospheric GCM. NASA Tech. Memo. 104606, Vol. 17, Goddard Space Flight Center, Greenbelt, MD, 194 pp.
- Barlow, M., S. Nigam, and E. H. Berbery, 2001: ENSO, Pacific decadal variability, and U.S. summertime precipitation, drought, and stream flow. *J. Climate*, **14**, 2105–2128, doi:10.1175/1520-0442(2001)014<2105:EPDVAU>2.0.CO;2.
- Barsugli, J., and P. D. Sardeshmukh, 2002: Global atmospheric sensitivity to tropical SST anomalies throughout the Indo-Pacific basin. *J. Climate*, **15**, 3427–3442, doi:10.1175/1520-0442(2002)015<3427:GASTTS>2.0.CO;2.
- Burgman, R., A. Clement, C. Mitas, J. Chen, and K. Esslinger, 2008a: Evidence for atmospheric variability over the Pacific on decadal timescales. *Geophys. Res. Lett.*, **35**, L01704, doi:10.1029/2007GL031830.
- , P. S. Schopf, and B. P. Kirtman, 2008b: Decadal modulation of ENSO in a hybrid coupled model. *J. Climate*, **21**, 5482–5500, doi:10.1175/2008JCLI1933.1.
- , R. Seager, A. Clement, and C. Herweijer, 2010: Role of tropical Pacific SSTs in global medieval hydroclimate: A modeling study. *Geophys. Res. Lett.*, **37**, L06705, doi:10.1029/2009GL042239.
- Campana, K., and P. Caplan, Eds., 2005: Technical procedures bulletin for the T382 Global Forecast System. [Available online at http://www.emc.ncep.noaa.gov/gc_wmb/Documentation/TPBOct05/T382.TPB.FINAL.htm.]
- Clement, A. C., R. Burgman, and J. R. Norris, 2009: Observational and model evidence for positive low-level cloud feedback. *Science*, **325**, 460–464, doi:10.1126/science.1171255.
- Delworth, T. L., and Coauthors, 2006: GFDL's CM2 global coupled climate models. Part I: Formulation and simulation characteristics. *J. Climate*, **19**, 643–674, doi:10.1175/JCLI3629.1.

- Deser, C., A. S. Phillips, and J. W. Hurrell, 2004: Pacific interdecadal climate variability: Linkages between the Tropics and the North Pacific during boreal winter since 1900. *J. Climate*, **17**, 3109–3124, doi:[10.1175/1520-0442\(2004\)017<3109:PICVLB>2.0.CO;2](https://doi.org/10.1175/1520-0442(2004)017<3109:PICVLB>2.0.CO;2).
- Enfield, D., A. M. Mestas-Nuñez, and P. J. Trimble, 2001: The Atlantic multidecadal oscillation and its relation to rainfall and river flows in the continental U.S. *Geophys. Res. Lett.*, **28**, 2077–2080, doi:[10.1029/2000GL012745](https://doi.org/10.1029/2000GL012745).
- Fedorov, A. V., and S. G. H. Philander, 2000: Is El Niño changing? *Science*, **288**, 1997–2002, doi:[10.1126/science.288.5473.1997](https://doi.org/10.1126/science.288.5473.1997).
- Findell, K. L., and T. L. Delworth, 2010: Impact of common sea surface temperature anomalies on global drought and pluvial frequency. *J. Climate*, **23**, 485–503, doi:[10.1175/2009JCLI3153.1](https://doi.org/10.1175/2009JCLI3153.1).
- Gates, W. L., and Coauthors, 1999: An overview of the results of the Atmospheric Model Intercomparison Project (AMIP I). *Bull. Amer. Meteor. Soc.*, **80**, 29–55, doi:[10.1175/1520-0477\(1999\)080<0029:AOOTRO>2.0.CO;2](https://doi.org/10.1175/1520-0477(1999)080<0029:AOOTRO>2.0.CO;2).
- Herweijer, C., and R. Seager, 2008: The global footprint of persistent extra-tropical drought in the instrumental era. *Int. J. Climatol.*, **28**, 1761–1774, doi:[10.1002/joc.1590](https://doi.org/10.1002/joc.1590).
- , —, and E. R. Cook, 2006: North American droughts of the mid to late nineteenth century: A history, simulation and implication for Mediaeval drought. *Holocene*, **16**, 159–171, doi:[10.1191/0959683606hl917rp](https://doi.org/10.1191/0959683606hl917rp).
- Higgins, R. W., Y. Yao, E. S. Yarosh, J. E. Janowiak, and K. C. Mo, 1997: Influence of the Great Plains low-level jet on summertime precipitation and moisture transport over the central United States. *J. Climate*, **10**, 481–507, doi:[10.1175/1520-0442\(1997\)010<0481:IOTGPL>2.0.CO;2](https://doi.org/10.1175/1520-0442(1997)010<0481:IOTGPL>2.0.CO;2).
- Hoerling, M., and A. Kumar, 2003: The perfect ocean for drought. *Science*, **299**, 691–694, doi:[10.1126/science.1079053](https://doi.org/10.1126/science.1079053).
- , —, and Coauthors, 2013: Anatomy of an extreme event. *J. Climate*, **26**, 2811–2832, doi:[10.1175/JCLI-D-12-00270.1](https://doi.org/10.1175/JCLI-D-12-00270.1).
- Hu, Q., and S. Feng, 2002: Interannual rainfall variations in the North American summer monsoon region: 1900–98. *J. Climate*, **15**, 1189–1202, doi:[10.1175/1520-0442\(2002\)015<1189:IRVITN>2.0.CO;2](https://doi.org/10.1175/1520-0442(2002)015<1189:IRVITN>2.0.CO;2).
- , —, and R. J. Oglesby, 2011: Variations in North American summer precipitation driven by the Atlantic multidecadal oscillation. *J. Climate*, **24**, 5555–5570, doi:[10.1175/2011JCLI4060.1](https://doi.org/10.1175/2011JCLI4060.1).
- Kirtman, B. P., and P. S. Schopf, 1998: Decadal variability of ENSO predictability and prediction. *J. Climate*, **11**, 2804–2822, doi:[10.1175/1520-0442\(1998\)011<2804:DVIEPA>2.0.CO;2](https://doi.org/10.1175/1520-0442(1998)011<2804:DVIEPA>2.0.CO;2).
- , —, and Coauthors, 2014: The North American Multimodel Ensemble: Phase-1 Seasonal-to-interannual prediction; Phase-2 toward developing intraseasonal prediction. *Bull. Amer. Meteor. Soc.*, **95**, 585–601, doi:[10.1175/BAMS-D-12-00050.1](https://doi.org/10.1175/BAMS-D-12-00050.1).
- Koster, R. D., and Coauthors, 2006: GLACE: The Global Land-Atmosphere Coupling Experiment. Part I: Overview. *J. Hydrometeor.*, **7**, 590–610, doi:[10.1175/JHM510.1](https://doi.org/10.1175/JHM510.1).
- Latif, M., and T. P. Barnett, 1994: Causes of decadal climate variability over the North Pacific and North America. *Science*, **266**, 634–637, doi:[10.1126/science.266.5185.634](https://doi.org/10.1126/science.266.5185.634).
- Mantua, N., S. R. Hare, Y. Zhang, J. M. Wallace, and R. C. Francis, 1997: A Pacific interdecadal climate oscillation with impacts on salmon production. *Bull. Amer. Meteor. Soc.*, **78**, 1069–1079, doi:[10.1175/1520-0477\(1997\)078<1069:APCOW>2.0.CO;2](https://doi.org/10.1175/1520-0477(1997)078<1069:APCOW>2.0.CO;2).
- McCabe, G. J., M. A. Palecki, and J. L. Betancourt, 2004: Pacific and Atlantic Ocean influences on multidecadal drought frequency in the United States. *Proc. Natl. Acad. Sci. USA*, **101**, 4136–4141, doi:[10.1073/pnas.0306738101](https://doi.org/10.1073/pnas.0306738101).
- McGregor, S., A. Timmermann, M. F. Stuecker, M. H. England, M. Merrifield, F.-F. Jin, and Y. Chikamoto, 2014: Recent Walker circulation strengthening and Pacific cooling amplified by Atlantic warming. *Nat. Climate Change*, **4**, 888–892, doi:[10.1038/nclimate2330](https://doi.org/10.1038/nclimate2330).
- Meehl, G. A., J. M. Arblaster, and C. Tebaldi, 2005: Understanding future patterns of increased precipitation intensity in climate model simulations. *Geophys. Res. Lett.*, **32**, L18719, doi:[10.1029/2005GL023680](https://doi.org/10.1029/2005GL023680).
- Mo, K., J. N. Paegle, and R. Higgins, 1997: Atmospheric processes associated with summer floods and droughts in the central United States. *J. Climate*, **10**, 3028–3046, doi:[10.1175/1520-0442\(1997\)010<3028:APAWSF>2.0.CO;2](https://doi.org/10.1175/1520-0442(1997)010<3028:APAWSF>2.0.CO;2).
- , J. E. Schemm, and S. You, 2009: Influence of ENSO and the Atlantic multidecadal oscillation on drought over the United States. *J. Climate*, **22**, 5962–5982, doi:[10.1175/2009JCLI2966.1](https://doi.org/10.1175/2009JCLI2966.1).
- Namias, J., 1955: Some meteorological aspects of drought. *Mon. Wea. Rev.*, **83**, 199–205, doi:[10.1175/1520-0493\(1955\)083<0199:SMAOD>2.0.CO;2](https://doi.org/10.1175/1520-0493(1955)083<0199:SMAOD>2.0.CO;2).
- Newman, M., G. P. Compo, and M. A. Alexander, 2003: ENSO-forced variability of the Pacific decadal oscillation. *J. Climate*, **16**, 3853–3857, doi:[10.1175/1520-0442\(2003\)016<3853:EVOTPD>2.0.CO;2](https://doi.org/10.1175/1520-0442(2003)016<3853:EVOTPD>2.0.CO;2).
- Nigam, S., M. Barlow, and E. H. Berbery, 1999: Analysis links Pacific decadal variability to drought and streamflow in the United States. *Eos, Trans. Amer. Geophys. Union*, **80**, 621–625, doi:[10.1029/99EO00412](https://doi.org/10.1029/99EO00412).
- Power, S., T. Casey, C. Folland, A. Colman, and V. Mehta, 1999: Inter-decadal modulation of the impact of ENSO on Australia. *Climate Dyn.*, **15**, 319–324, doi:[10.1007/s003820050284](https://doi.org/10.1007/s003820050284).
- Rayner, N. A., D. E. Parker, E. B. Horton, C. K. Folland, L. V. Alexander, D. P. Rowell, E. C. Kent, and A. Kaplan, 2003: Global analyses of SST, sea ice, and night marine air temperature since the late nineteenth century. *J. Geophys. Res.*, **108**, 4407, doi:[10.1029/2002JD002670](https://doi.org/10.1029/2002JD002670).
- Ropelewski, C. F., and M. S. Halpert, 1986: North American precipitation and temperature patterns associated with the El Niño/Southern Oscillation (ENSO). *Mon. Wea. Rev.*, **114**, 2352–2362, doi:[10.1175/1520-0493\(1986\)114<2352:NAPATP>2.0.CO;2](https://doi.org/10.1175/1520-0493(1986)114<2352:NAPATP>2.0.CO;2).
- Schopf, P. S., and R. J. Burgman, 2006: A simple mechanism for ENSO residuals and asymmetry. *J. Climate*, **19**, 3167–3179, doi:[10.1175/JCLI3765.1](https://doi.org/10.1175/JCLI3765.1).
- Schubert, S. D., M. J. Suarez, P. J. Pegion, M. A. Kistler, and A. Kumar, 2002: Predictability of zonal means during boreal summer. *J. Climate*, **15**, 420–434, doi:[10.1175/1520-0442\(2002\)015<0420:POZMDB>2.0.CO;2](https://doi.org/10.1175/1520-0442(2002)015<0420:POZMDB>2.0.CO;2).
- , —, —, —, R. D. Koster, and J. T. Bacmeister, 2004a: Causes of long-term drought in the U.S. Great Plains. *J. Climate*, **17**, 485–503, doi:[10.1175/1520-0442\(2004\)017<0485:COLDIT>2.0.CO;2](https://doi.org/10.1175/1520-0442(2004)017<0485:COLDIT>2.0.CO;2).
- , —, —, —, and —, 2004b: On the cause of the 1930s Dust Bowl. *Science*, **303**, 1855–1859, doi:[10.1126/science.1095048](https://doi.org/10.1126/science.1095048).
- , —, and Coauthors, 2009: A U.S. CLIVAR project to assess and compare the responses of global climate models to drought-related SST forcing patterns: Overview and results. *J. Climate*, **22**, 5251–5272, doi:[10.1175/2009JCLI3060.1](https://doi.org/10.1175/2009JCLI3060.1).
- Seager, R., N. Harnik, Y. Kushnir, W. Robinson, and J. Miller, 2003: Mechanisms of hemispherically symmetric climate variability. *J. Climate*, **16**, 2960–2978, doi:[10.1175/1520-0442\(2003\)016<2960:MOHSCV>2.0.CO;2](https://doi.org/10.1175/1520-0442(2003)016<2960:MOHSCV>2.0.CO;2).
- , Y. Kushnir, C. Herweijer, N. Naik, and J. Velez, 2005: Modeling of tropical forcing of persistent droughts and

- pluvials over western North America: 1856–2000. *J. Climate*, **18**, 4065–4088, doi:[10.1175/JCLI3522.1](https://doi.org/10.1175/JCLI3522.1).
- , and Coauthors, 2007: Model projections of an imminent transition to a more arid climate in southwestern North America. *Science*, **316**, 1181–1184, doi:[10.1126/science.1139601](https://doi.org/10.1126/science.1139601).
- , R. Burgman, Y. Kushnir, A. Clement, E. Cook, N. Naik, and J. Miller, 2008: Tropical Pacific forcing of North American medieval megadroughts: Testing the concept with an atmosphere model forced by coral-reconstructed SSTs. *J. Climate*, **21**, 6175–6190, doi:[10.1175/2008JCLI2170.1](https://doi.org/10.1175/2008JCLI2170.1).
- , N. Naik, M. Ting, M. A. Cane, N. Harmik, and Y. Kushnir, 2010: Adjustment of the atmospheric circulation to tropical Pacific SST anomalies: Variability of transient eddy propagation in the Pacific–North America sector. *Quart. J. Roy. Meteor. Soc.*, **136**, 277–296, doi:[10.1002/qj.588](https://doi.org/10.1002/qj.588).
- Thompson, D. W. J., and J. M. Wallace, 1998: The Arctic Oscillation signature in the wintertime geopotential height and temperature fields. *Geophys. Res. Lett.*, **25**, 1297–1300, doi:[10.1029/98GL00950](https://doi.org/10.1029/98GL00950).
- Trenberth, K. E., and C. J. Guillemot, 1996: Physical processes involved in the 1988 drought and 1993 floods in North America. *J. Climate*, **9**, 1288–1298, doi:[10.1175/1520-0442\(1996\)009<1288:PPITD>2.0.CO;2](https://doi.org/10.1175/1520-0442(1996)009<1288:PPITD>2.0.CO;2).
- , G. W. Branstator, and P. A. Arkin, 1988: Origins of the 1988 North American drought. *Science*, **242**, 1640–1645, doi:[10.1126/science.242.4886.1640](https://doi.org/10.1126/science.242.4886.1640).
- , —, D. Karoly, A. Kumar, N.-C. Lau, and C. Ropelewski, 1998: Progress during TOGA in understanding and modeling global teleconnections associated with tropical sea surface temperatures. *J. Geophys. Res.*, **103**, 14 291–14 324, doi:[10.1029/97JC01444](https://doi.org/10.1029/97JC01444).
- Wang, H., S. Schubert, M. Suarez, and R. Koster, 2010: The physical mechanism by which the leading patterns of SST variability impact U.S. precipitation. *J. Climate*, **23**, 1815–1836, doi:[10.1175/2009JCLI3188.1](https://doi.org/10.1175/2009JCLI3188.1).
- Woodhouse, C. A., and J. T. Overpeck, 1998: 2000 years of drought variability in the central United States. *Bull. Amer. Meteor. Soc.*, **79**, 2693–2714, doi:[10.1175/1520-0477\(1998\)079<2693:YODVIT>2.0.CO;2](https://doi.org/10.1175/1520-0477(1998)079<2693:YODVIT>2.0.CO;2).
- Wu, R., and J. L. Kinter III, 2009: Analysis of the relationship of U.S. droughts with SST and soil moisture: Distinguishing the time scale of droughts. *J. Climate*, **22**, 4520–4538, doi:[10.1175/2009JCLI2841.1](https://doi.org/10.1175/2009JCLI2841.1).
- Yin, J. H., 2005: A consistent poleward shift of the storm tracks in simulations of 21st century climate. *Geophys. Res. Lett.*, **32**, L18701, doi:[10.1029/2005GL023684](https://doi.org/10.1029/2005GL023684).
- Yu, J.-Y., Y. Zou, S. T. Kim, and T. Lee, 2012: The changing impact of El Niño on US winter temperatures. *Geophys. Res. Lett.*, **39**, L15702, doi:[10.1029/2012GL052483](https://doi.org/10.1029/2012GL052483).
- Zhang, Y., J. M. Wallace, and D. Battisti, 1997: ENSO-like interdecadal variability: 1900–93. *J. Climate*, **10**, 1004–1020, doi:[10.1175/1520-0442\(1997\)010<1004:ELIV>2.0.CO;2](https://doi.org/10.1175/1520-0442(1997)010<1004:ELIV>2.0.CO;2).